Deuterium hyperfine splittings in the rotational spectrum of NH2D as revealed by Lamb-dip spectroscopy

Deuterium hyperfine splittings in the rotational spectrum of NH_2D as revealed by Lamb-dip spectroscopy

Mattia Melosso[a], Luca Dore[a,*], Jürgen Gauss[b], Cristina Puzzarini[a]

[a] *Dipartimento di Chimica "Giacomo Ciamician", Università di Bologna, Via F. Selmi 2, 40126 Bologna (Italy)*
[b] *Department Chemie, Johannes Gutenberg - Universität Mainz Duesbergweg 10–14, 55128 Mainz (Germany)*

Abstract

In the context of radio-astronomical observations, laboratory experiments constitute a cornerstone in the interpretation of rich line surveys due to the concomitant presence of numerous emitting molecules. Here, we report the investigation of three different rotational transitions of monodeuterated ammonia (NH_2D), a species of astrophysical interest, for which the contribution of the deuterium nuclear spin to the rotational spectrum has been resolved for the first time in the millimeter- and submillimeter-wave domain. The effect of hyperfine interactions on the rotational spectrum has been unveiled by a combined theoretical and experimental approach.

Quantum-chemical calculations based on coupled-cluster theory have been employed to evaluate the hyperfine parameters of nitrogen, hydrogen, and deuterium in NH_2D. Subsequently, the Lamb-dip technique has been used to investigate the rotational spectrum of NH_2D at high-resolution. In detail, three low-J transitions have been recorded at 86, 110, and 333 GHz with a frequency-modulation millimeter-/submillimeter-wave spectrometer. From the line profile analysis of the recorded spectra, the main terms responsible for the rotational hyperfine structure have been determined with good accuracy.

Our work allows a comprehensive analysis of the rotational features of NH_2D in radioastronomical spectra and a more accurate evaluation of its column density, especially in non-turbulent regions showing narrow linewidths.

Keywords: Lamb-dip technique, Hyperfine structure, Quantum-chemical calculations, Ammonia, Interstellar medium, Deuterium fractionation

1. Introduction

Ammonia (NH_3) has been one of the first molecules observed in the interstellar medium (ISM) [1]: its detection contributed to the birth of astrochemistry as we know it today. Since then, the number of interstellar molecules has been increasing continuously. The current census accounts for more than 200 different species discovered in the ISM and circumstellar shells, and most of them have been detected thanks to their rotational features [2]. To contribute to new detections as well as to accurately derive molecular abundances, laboratory efforts dedicated to the study of molecules of astrophysical interest are fundamental. Besides the fascination of a new molecule identified in the ISM, astrochemical observations are crucial to constrain chemical models in astronomy. Deuterium fractionation processes, for instance, are of great importance in tracing evolutionary stages during the formation of a Sun-like star [3]. Deuterated ammonia is known to be relatively abundant in the ISM. NH_2D transitions have been first observed towards the Orion nebula [4] and the giant molecular cloud Sagittarius B2 [5]. Later, NH_2D has been observed in prestellar cores, low- and high-mass star-forming regions, hot core, cold molecular clouds, and many other objects [6, 7, 8, 9].

*Corresponding author
Email address: luca.dore@unibo.it (Luca Dore)

Two rotational transitions in the 3 mm band are usually used to detect NH_2D and to derive the deuterium fractionation (D/H) of ammonia. These lines correspond to the $J_{Ka,\,Kc} = 1_{1,1} - 1_{0,1}$ transitions of *ortho*- (at 86 GHz) and *para*-NH_2D (at 110 GHz). Typically, the observed linewidths are sufficiently narrow to resolve the hyperfine structure caused by the nitrogen quadrupole coupling, and thus to properly estimate the column density of NH_2D. However, recent observations of monodeuterated ammonia with the IRAM 30m and APEX telescopes have pointed out that the hyperfine splittings due to deuterium may affect the analysis of NH_2D features and, consequently, its column density [10]. Indeed, the discrepancies between observed and expected linewidths of the $1_{1,1} - 1_{0,1}$ and $1_{0,1} - 0_{0,0}$ transitions in the starless core H-MM1 could only be explained with the inclusion of the deuterium hyperfine structure. Unfortunately, to date, laboratory studies of NH_2D have never taken into account the effect of deuterium hyperfine interactions for those transitions.

The investigation of the microwave spectrum of monodeuterated ammonia started in the 50s and 60s with Stark effect [11] and maser spectroscopy measurements [12, 13], but the first thorough analysis of the rotation-inversion spectrum of NH_2D was carried out in the following decade by De Lucia & Helminger [14], who recorded several transitions in the millimeter- and submillimeter-wave domains. The analysis of the NH_2D spectrum has been subsequently extended by the observation of nitrogen quadrupole resolved [15, 16] and higher-J transitions [15, 17].

Here, we report the Lamb-dip spectra of three NH_2D transitions observed at millimeter-/submillimeter-wavelengths, for which deuterium hyperfine splittings have been resolved for the first time. The experimental work has been supported by state-of-the-art quantum-chemical calculations, which were used to evaluate the nuclear quadrupole coupling (NQC), spin-rotation (SR), and dipolar spin-spin (SS) tensors of NH_2D.

The structure of this paper is organized as follows. First, the complexity of the NH_2D spectrum is presented and the Hamiltonian described (§2). Second, the computational details employed in the evaluation of the hyperfine parameters are reported (§3). Then, the experimental details are given together with the main results (§4) and, finally, concluding remarks –with some emphasis on the astrophysical implications of this work– are reported (§5).

2. Spectral analysis

Monodeuterated ammonia, NH_2D, is an asymmetric-top rotor, which –like its parent species NH_3– tunnels between two equivalent configurations passing through a planar transition state: its molecular symmetry group is the $C_{2v}(M)$ (see Figure 1). The main effect of this inversion motion is the splitting of each $J_{K_a,\,K_c}$ rotational level into two sub-levels, one symmetric (s, A_1) and the other anti-symmetric (a, B_1) with respect to inversion, the energy splitting for the $0_{0,0}$ levels being $\Delta E = 12.169438(5)$ GHz. The permanent dipole moment in NH_2D ($\mu = 1.474$ D) is distributed along two components, μ_a=-0.18 D (A_1 symmetry) and μ_c=1.463 D (B_1) [15]. Therefore, a-type transitions are pure rotational, whereas μ_c-allowed transitions connect inversion states of different symmetry.

The hyperfine structure of the NH_2D rotational spectrum is the result of several interactions. In the present case, all nuclei (^{14}N, D and H) have non-zero nuclear spin (I) and thus contribute to the hyperfine structure. The presence of two equivalent hydrogen nuclei leads to the existence of *ortho* and *para* species, and the total nuclear spin, $I_{\rm H,tot} = I_{\rm H_1} + I_{\rm H_2}$, needs to be considered. The *ortho* species corresponds to $I_{\rm H,tot} = 1$, with three spin functions of A_1 symmetry, whereas the *para* form is characterized by $I_{\rm H,tot} = 0$, with one spin function of B_2 symmetry. In addition, the symmetry of the asymmetric-top states, denoted by the parity of K_a and K_c, is: A_1 for even, even (ee), A_2 for eo, B_1 for oo, and B_2 for oe. In conclusion, since the total wavefunction has to be of B symmetry, namely antisymmetric with respect to the exchange of the two H nuclei, the *ortho* form has rotation-inversion states of the type (s, oo), (s, oe), (a, ee), and (a, eo), while for the *para* form holds (s, ee), (s, eo), (a, oo), and (a, oe). Thus *ortho* and *para* species have similar spectra, with the former stronger because of spin statistics.

Having $I = 1$, nitrogen and deuterium are quadrupolar nuclei, and thus the hyperfine interactions involved are the quadrupole coupling and the spin-rotation interaction. For hydrogen, the nuclear spin is $I_{\rm H}$=1/2, and thus only the spin-rotation interaction occurs. In addition, the dipolar spin-spin couplings between the possible nuclear spin pairs, namely N-D, N-H, H-H and D-H, should be considered.

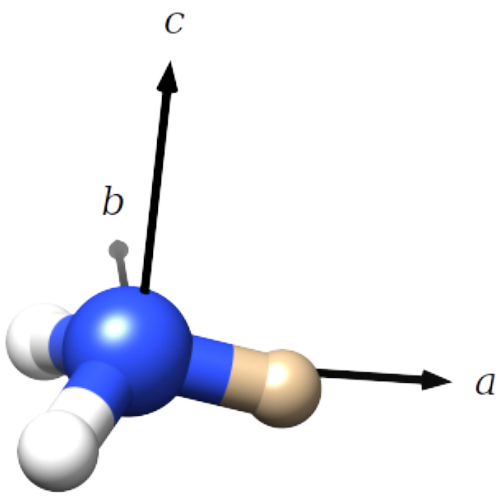

Figure 1: Monodeuterated ammonia NH_2D in its principal inertia system. The hydrogen atoms are depicted in white, while deuterium is in tan.

The Hamiltonian used in the analysis of the retrieved hyperfine component frequencies consists of four different contributions:

$$\mathbf{H} = \mathbf{H}_{\mathrm{ROT}} + \mathbf{H}_{\mathrm{NQC}} + \mathbf{H}_{\mathrm{SR}} + \mathbf{H}_{\mathrm{SS}} \,, \tag{1}$$

where $\mathbf{H}_{\mathrm{ROT}}$ is the rotational part of the Hamiltonian operator [18]. $\mathbf{H}_{\mathrm{NQC}}$ describes the nuclear quadrupole couplings, $\mathbf{H}_{\mathrm{SR}}$ is the Hamiltonian describing the spin-rotation interactions, and $\mathbf{H}_{\mathrm{SS}}$ describes the spin-spin couplings due to direct dipolar interactions.
The angular momentum coupling scheme adopted is:

$$\mathbf{F}_1 = \mathbf{J} + \mathbf{I}_{\mathrm{N}} \,, \qquad \mathbf{F}_2 = \mathbf{F}_1 + \mathbf{I}_{\mathrm{D}} \,, \qquad \mathbf{F} = \mathbf{F}_2 + \mathbf{I}_{\mathrm{H,tot}} \,. \tag{2}$$

3. Computational details

For the accurate computation of hyperfine parameters, quantum-chemical calculations are based on the coupled-cluster (CC) theory [19] for the treatment of the electron correlation. The CC singles and doubles (CCSD) approach augmented by a perturbative treatment of triple excitations (CCSD(T)) [20] has been used in conjunction with a hierarchic series of correlation consistent basis sets (the aug-cc-pCVnZ, with n = D-6, basis sets [21, 22, 23, 24, 25]) in order to exploit the extrapolation to the complete basis set (CBS) limit. To further improve the accuracy of the computed hyperfine parameters, the contributions due to the full treatment of triple and quadruple excitations have also been considered. While the CCSD(T) computations have been performed using the CFOUR program package [26], the CC singles, doubles and triples, CCSDT [27, 28], and CC with singles, doubles, triples, quadruples, CCSDTQ [29], calculations have been carried out using the MRCC program [30] interfaced to the CFOUR package. In detail, the composite scheme employed, which involves only computations with all electron correlated (all), can be summarized as follows:

$$p_{best} = p^{\infty}(\mathrm{HF-SCF}) + \Delta p^{\infty}(\mathrm{CCSD(T)}) + \Delta p(\mathrm{fT}) + \Delta p(\mathrm{fQ}) \,, \tag{3}$$

where p denotes a generic hyperfine parameter. The CBS limit has been obtained by means of a two-step procedure by extrapolating separately the Hartree-Fock self-consistent-field (HF-SCF) part with the exponential expression by Feller [31], applied to the aug-cc-pCVnZ basis sets with n = Q, 5, and 6, and the CCSD(T) correlation contribution with the n^{-3} extrapolation scheme [32], with the n=5 and 6 sets chosen for the purpose. Corrections due to a full treatment of triples (fT) and to quadruples (fQ) have been

evaluated as differences between CCSDT and CCSD(T) and between CCSDTQ and CCSDT calculations, respectively. The aug-cc-pCVTZ basis set has been used for the fT term, whereas aug-cc-pCVDZ has been employed for the fQ correction.

Computations of hyperfine parameters have been carried out at the equilibrium geometry obtained by resorting to the so-called composite "gradient" scheme [33, 34]. The equilibrium structure has been determined by minimizing the following energy gradient:

$$\frac{dE_{\rm best}}{dx} = \frac{dE^{\infty}({\rm HF-SCF})}{dx} + \frac{d\Delta E^{\infty}({\rm CCSD(T)})}{dx} + \frac{d\Delta E(core)}{dx} + \frac{d\Delta E({\rm fT})}{dx} + \frac{d\Delta E({\rm fQ})}{dx} \ . \qquad (4)$$

The extrapolation to the CBS limit is analogous to that performed in Eq. (3), with different basis sets employed, i.e., the cc-pVnZ family with n=Q,5, and 6 have been chosen for the HF-SCF extrapolation as well n=5 and 6 for the CCSD(T) valence correlation energy. The third term on the right-hand side of the equation above allows for incorporating the core-correlation effects as difference of all-electron and frozen-core CCSD(T) calculations using the cc-pCV5Z set. The last two terms are the fT and fQ contributions, which –as done for the extrapolation to the CBS limit– have been evaluated within the frozen-core approximation using the cc-pVTZ and cc-pVDZ basis sets, respectively.

For a quantitative prediction of the hyperfine parameters, the equilibrium values need to be augmented by vibrational corrections. For the evaluation of the latter, the approach employed is based on second-order vibrational perturbation theory (VPT2) [35]. The VPT2 approach is described in detail in Ref. [36] and is well-tested for the computation of vibrational corrections to hyperfine parameters (see, for example, Refs. [37, 38, 39, 40, 41, 42]). Vibrational corrections have been computed at the CCSD(T)/aug-cc-pCVQZ level with all electrons correlated. Subsequently, these corrections have been added to the best-estimated equilibrium results to derive values that can be directly compared to experiment or can be used to guide the spectral analysis and the fitting procedure.

The main focus of the present calculations is on the determination of the NQC, SR, and SS interaction constants. While we refer interested readers to, e.g., Ref. [43] for a detailed account on how hyperfine parameters can be obtained by means of quantum-chemical computations, in the following, we briefly summarize the relevant information. For quadrupolar nuclei (^{14}N and D in the present case), the nuclear quadrupole-coupling constants χ_{ij} have been obtained by the following expression:

$$\chi_{ij} = eQq_{ij}, \qquad (5)$$

where i and j refer to the inertial axes. eQ is the quadrupole moment (20.44(3) mbarn for ^{14}N and 2.860(15) mbarn for D [44]), and q_{ij} represents the ij-th element of the electric-field gradient tensor [18, 43]. The latter is the quantity that needs to be quantum-chemically computed. As a first-order property, its computation has been accomplished in a straightforward manner by means of analytic-gradient techniques [45].

While a detailed account on quantum-chemical calculations of the nuclear SR tensors $\mathbf{C}$ can be found in Refs. [46, 47], here, we limit ourselves to note that the electronic contribution of $\mathbf{C}$ is evaluated as the second derivative of the electronic energy with respect to the rotational angular momentum and the nuclear spin [46, 48, 47] in conjunction with perturbation-dependent basis functions [46] (also referred to as rotational London orbitals) to improve the basis-set convergence. The nuclear contribution, instead, only depends on the molecular geometry (see, e.g., Ref. [49] and references therein), and the same applies to the dipolar spin-spin coupling tensor $\mathbf{D}$, for which expressions can be found, for instance, in Refs. [18, 43, 50].

The computed values of all NQC, SR, and SS interaction constants are listed in Table 1.

4. Experiment and Results

Spectral recordings were performed with a frequency-modulation (FM) submillimeter spectrometer, employed in the past for the study of other deuterated species [51, 52, 53, 54] and Lamb-dip measurements (see, e.g., Refs. [40, 41, 55, 56]). A Gunn diode (J.E. Carlstrom Co) emitting in the 80–115 GHz range is used as radiation source; spectral coverage of the $1_{0,1} - 0_{0,0}$ transition around 333 GHz is obtained by

Table 1: Computed nuclear quadrupole, spin-rotation, and dipolar spin-spin coupling constants of NH_2D.

Parameter	Atom	Unit	Value
χ_{aa}	(N)	MHz	1.8986
χ_{cc}	(N)	MHz	−3.9555
χ_{ac}	(N)	MHz	0.9390
C_{aa}	(N)	kHz	6.967
C_{bb}	(N)	kHz	4.426
C_{cc}	(N)	kHz	5.067
χ_{aa}	(D)	MHz	0.2405
χ_{cc}	(D)	MHz	−0.1293
χ_{ac}	(D)	MHz	−0.1110
C_{aa}	(D)	kHz	−0.1252
C_{bb}	(D)	kHz	−3.154
C_{cc}	(D)	kHz	−2.389
C_{aa}	(H)	kHz	25.599
C_{bb}	(H)	kHz	6.936
C_{cc}	(H)	kHz	13.165
D_{aa}	(N-D)	kHz	1.093
D_{cc}	(N-D)	kHz	1.290
D_{aa}	(N-H)	kHz	3.470
D_{cc}	(N-H)	kHz	−7.852
D_{aa}	(D-H)	kHz	4.075
D_{cc}	(D-H)	kHz	1.078
D_{aa}	(H-H)	kHz	28.080
D_{cc}	(H-H)	kHz	−56.160

Notes: Equilibrium values obtained using Eq. (3) augmented by vibrational corrections at the all-CCSD(T)/aug-cc-pCVQZ level. The nuclear quadrupole (χ_{ii}) and dipolar spin-spin coupling (D_{ii}) tensors have zero trace; thus, only two of the three diagonal components are given.

coupling the Gunn diode to a passive frequency multiplier (Virginia Diodes, WR3.4x3). A 75 MHz sine-wave modulated wave is used as reference signal in a Phase-Lock Loop (PLL) through which the Gunn's radiation is locked to one harmonic of a digital synthesizer (HP8672A, 2–18 GHz). Frequency accuracy is achieved by locking the radio-frequency synthesizers to a 5 MHz rubidium atomic clock. An indium antimonide (InSb) hot-electron bolometer cooled down to liquid-helium temperature (QMC Instr. Ltd. type QFI/2) is used as detector. The detector output is then demodulated at twice the modulation frequency f through an analog lock-in amplifier, so that the second derivative of the actual absorption spectrum is recorded. An additional signal-to-noise (S/N) improvement is achieved by filtering the signal into an Ohmic RC circuit. The lock-in signal is finally analog-to-digital converted and sent to a computer.

The optical elements of the spectrometer were appropriately set up in a double-pass configuration to perform Lamb-dip measurements [57], as previously done for the parent species NH_3 [55]. A wire grid polarizer was placed in front of the high-density polyethylene window of the absorption cell at 45° along the path of the incoming radiation, while a roof-top mirror was placed at the end of the cell in order to reflect back the

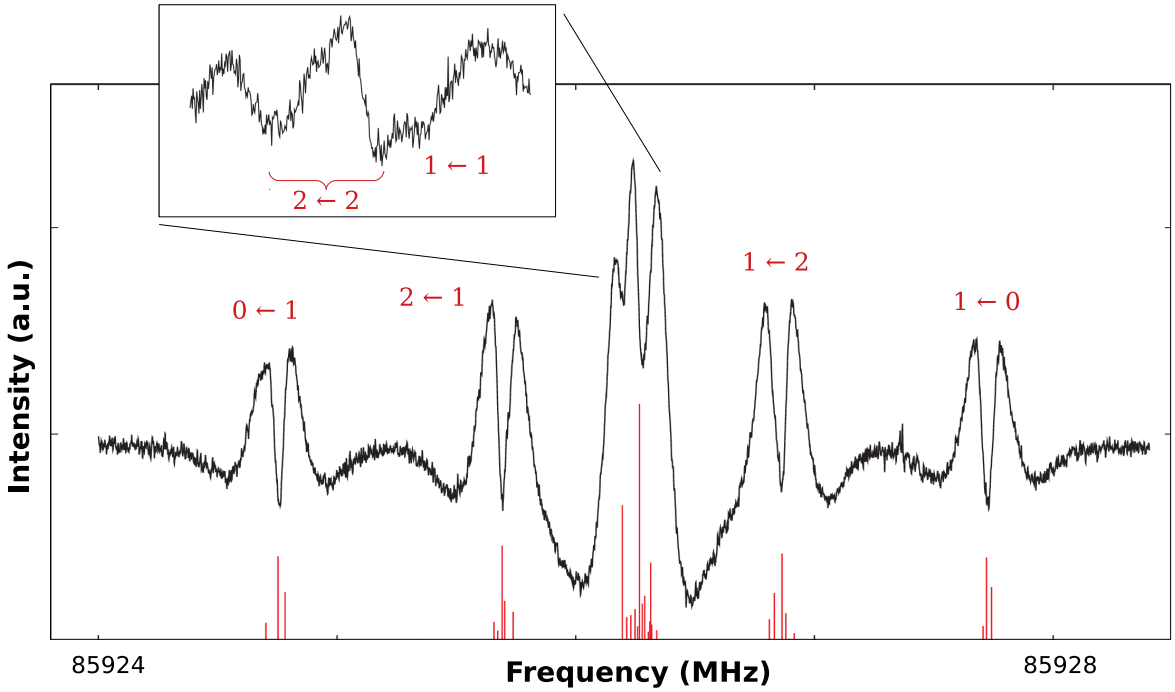

Figure 2: Lamb-dip spectrum of the *ortho*-NH_2D $1_{1,1} - 1_{0,1}$ transition showing nitrogen and deuterium hyperfine structure. The numbers above each hfs components refer to the $F_1' \leftarrow F_1$ quantum numbers. The magnified window shows the splittings due to deuterium quadrupolar interaction, as unveiled at higher-resolution experimental conditions. Red sticks represent the position and the intensity of each transition as predicted from our best spectroscopic parameters.

incoming radiation with its polarization rotated by 90°. The back beam is then reflected by the polarizer into the detector off-axes of 90°.

In addition to the double-pass arrangement, Lamb-dip measurements require a low-pressure regime, low f and modulation-depth values, and enough source power to partially saturate the transition. To record the spectra, monodeuterated ammonia was formed *in situ*, by flowing a small amount of NH_3 (< 0.5 mTorr) in the absorption cell where deuterium (D_2) had been previously discharged for some minutes. A frequency modulation of 1 kHz and modulation-depth values between 8 and 24 kHz were used to record the spectra.

These experimental conditions allowed to reveal both nitrogen and deuterium hyperfine splittings for three different rotational transitions of NH_2D. Figures 2 and 3 show the $J_{Ka,\,Kc} = 1_{1,1} - 1_{0,1}$ transitions of *ortho*- and *para*-NH_2D, respectively. Because of nitrogen quadrupolar interactions, each transition appears as a well-resolved quintet, with splittings of order of few hundreds kHz. On the other hand, deuterium quadrupole splittings are less pronounced, i.e., at least one order of magnitude smaller. Nonetheless, the deuterium hyperfine structure could be partially resolved, as shown in the magnified boxes of Figures 2 and 3.

Figure 4 illustrates the $J_{Ka,\,Kc} = 1_{0,1} - 0_{0,0}$ transition of NH_2D, which has been exclusively recorded for the *ortho* state (the same transition for the *para* state is weaker for spin-statistics reasons and could not be saturated in our experimental conditions). The transition appears as a well-resolved triplet, because only the $F_1 = 1$ level can exist for the lower state. The deuterium hyperfine structure is also less complicated and has been partly resolved for the middle component of the triplet. Moreover, two crossover resonances (also denoted as ghost transitions), marked with green asterisks, are evident in the spectrum of Figure 4. These dips are due to the saturation of overlapping Gaussian profiles of two transitions with a common energy level. Since they occur midway between the "interacting" transition frequencies, they offer additional information for data analysis.

To analyze the recorded spectra, first of all, the hyperfine structure of the NH_2D rotational spectrum

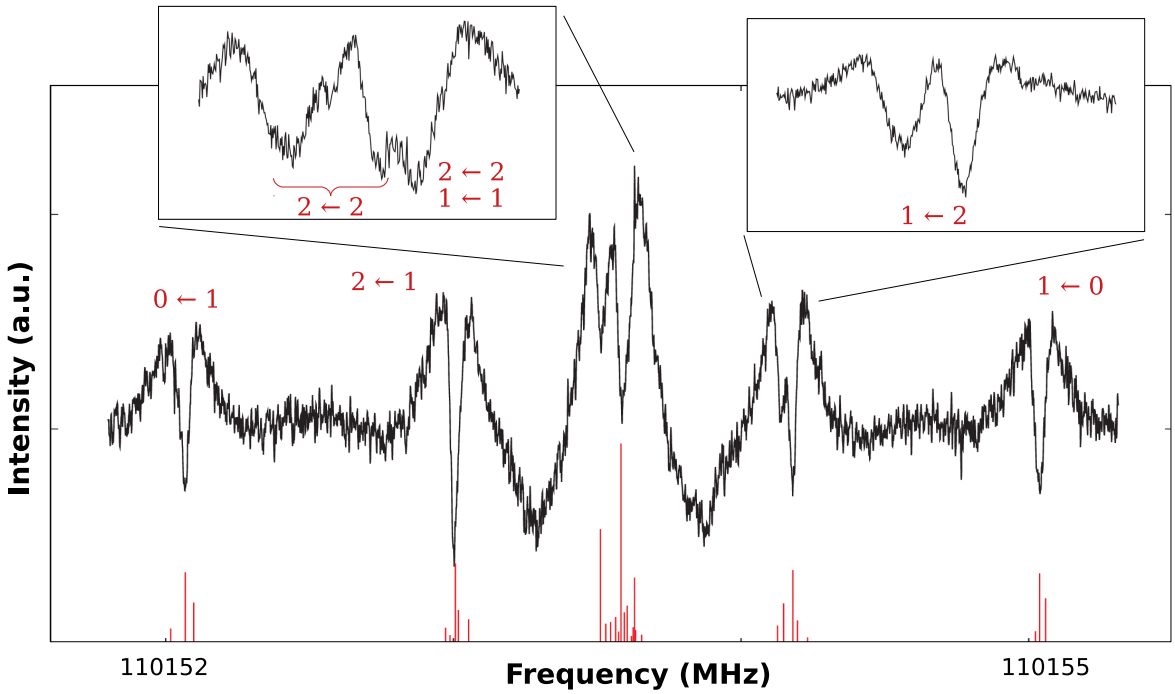

Figure 3: Lamb-dip spectrum of the *para*-NH_2D $1_{1,1} - 1_{0,1}$ transition showing nitrogen and deuterium hyperfine structure. The numbers above each hfs components refer to the $F_1' \leftarrow F_1$ quantum numbers. The magnified windows show the splittings due to deuterium quadrupolar interaction, as unveiled in higher-resolution experimental conditions. Red sticks represent the position and the intensity of each transition as predicted from our best spectroscopic parameters.

was predicted using the computed hyperfine constants (as explained in §3) together with experimental spectroscopic parameters (A, B, C, and so on) from previous works [15, 17]. The computed hyperfine constants turned out to be rather good and allowed us to easily assign each dip to the correct hyperfine component (or group of components). Then, the rest frequency of each line has been retrieved by modelling the recorded absorption profile using the proFFiT line analysis code [58].

Eventually, the newly observed transition frequencies of NH_2D (including ghost features) have been fitted along with literature data to the Hamiltonian of Equation (1). The least-squares procedure, in which each datum has been weighted proportionally to the inverse square of its uncertainty, has been performed with the SPFIT suite of program [59]. As far as the centrifugal analysis of NH_2D is concerned, most of the spectroscopic parameters have been determined with an accuracy comparable to that of previous works [15, 17]; for this reason, they are not reported here. Indeed, the focus and the major accomplishment of this work are the accurate determination of the diagonal NQC constants, χ_{ii}, and the C_{cc} SR constant of nitrogen and deuterium nuclei, which are collected in Table 2. The χ_{ii} terms of the hyperfine Hamiltonian are the main responsible of the actual splittings observed in the recorded spectra, which are typically revealed only in low-J transitions. Spin-rotation and spin-spin coupling interactions, instead, produce a shift in the energy levels that is difficult to determine without a larger set of hyperfine-resolved data. In our analysis, most SR constants and all the SS parameters have been kept fixed at the computed values of Table 1.

The new experimental transition frequencies are listed in Table 3 together with their residual errors from the global fit.

5. Conclusions

The hyperfine structure of the rotational spectrum of NH_2D has been investigated by combining high-level quantum-chemical calculations and high-resolution rotational spectroscopy. This work was motivated by

Table 2: Nitrogen and deuterium hyperfine constants determined for NH_2D.

Parameter	Unit	Atom	This work	Ref. [10]	Computed
χ_{aa}	MHz	(N)	1.9145(14)	1.906(84)	1.8986
χ_{cc}	MHz	(N)	−3.9470(12)	−3.95(13)	−3.9555
C_{cc}	kHz	(N)	4.94(13)		5.067
χ_{aa}	MHz	(D)	0.2229(67)	0.275[(a)]	0.2405
χ_{cc}	MHz	(D)	−0.1348(16)	−0.160(2)	−0.1293
C_{cc}	kHz	(D)	−2.266(97)		−2.389

Notes: Numbers in parenthesis are standard errors and apply to the last significant digits. (a) Fixed in the analysis.

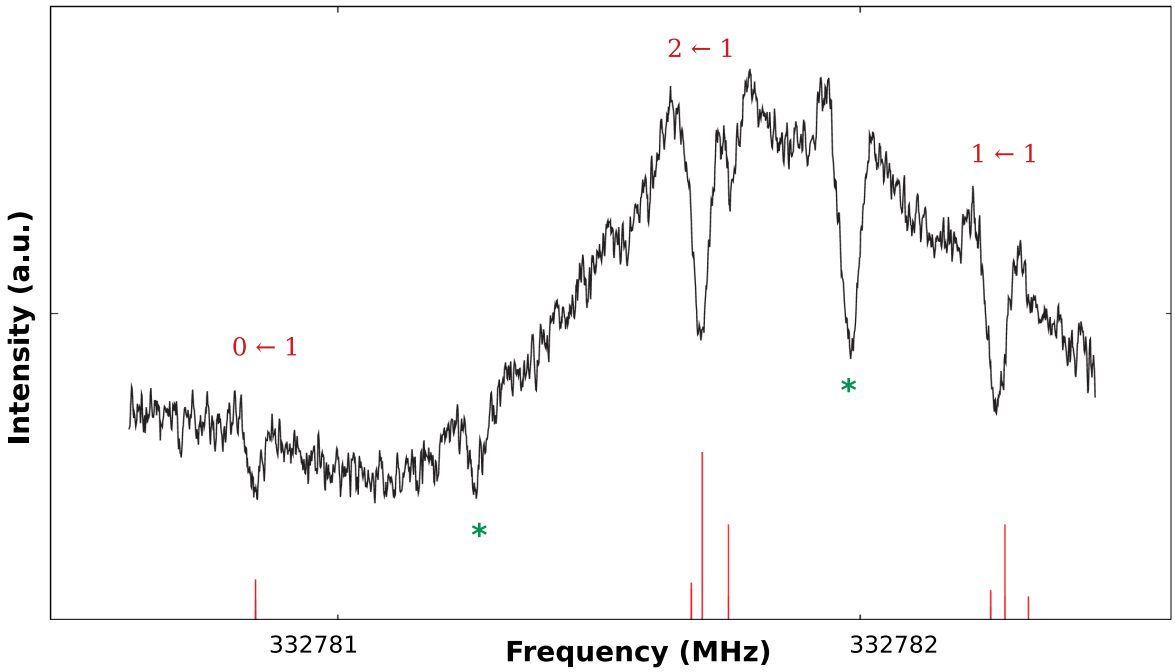

Figure 4: Lamb-dip spectrum of the *ortho*-NH_2D $1_{0,1} - 0_{0,0}$ transition showing nitrogen and deuterium hyperfine structure. The numbers above each hfs components refer to the $F_1' \leftarrow F_1$ quantum numbers, while ghost transitions are marked with green asterisks. Red sticks represent the position and the intensity of each transition as predicted from our best spectroscopic parameters.

the recent astronomical observation of NH_2D toward the dense core H-MM1 in Ophiuchus [10], where the rotational features show line-widths due to non-thermal motions that are sufficiently narrow to be affected by the small broadening caused by deuterium hyperfine splittings.

An highly accurate composite scheme has been employed to compute nitrogen, hydrogen, and deuterium hyperfine parameters, namely the NQC, SR, and SS interaction constants. Subsequently, three NH_2D rotational transitions have been recorded using the Lamb-dip technique, thus allowing not only the resolution of the nitrogen hyperfine structure, but also splittings due to deuterium. From the analysis of the newly observed transition frequencies, reliable values for the diagonal NQC constants and some SR parameters of both N and D have been derived. As can be seen from Table 2, the accuracy of χ_{aa}(N) and χ_{cc}(N)

Table 3: Measured hyperfine component frequencies of NH_2D.

Upper state					Lower state							
J'	K'_a	K'_c	F'_1	F'_2 [a]	J	K_a	K_c	F_1	F_2 [a]		Frequency (MHz)	Obs.-Calc.[b] (MHz)
					o-NH_2D							
1	1	1	0		1	0	1	1			85924.756	-0.001
1	1	1	2		1	0	1	1			85925.695	0.001
1	1	1	2	2	1	0	1	2	2		85926.197	-0.006
1	1	1	2	3	1	0	1	2	3	}	85926.271	-0.003
1	1	1	2	2	1	0	1	2	1	}		
1	1	1	1		1	0	1	1		}	85926.298	-0.004
1	1	1	2	1	1	0	1	2	1	}		
1	1	1	1		1	0	1	2			85926.862	-0.005
1	1	1	1		1	0	1	0			85927.725	0.005
					p-NH_2D							
1	1	1	0		1	0	1	1			110152.066	-0.002
1	1	1	2		1	0	1	1			110153.003	-0.002
1	1	1	2	2	1	0	1	2	2		110153.517	0.003
1	1	1	2	3	1	0	1	2	3	}	110153.581	-0.005
1	1	1	2	2	1	0	1	2	1	}		
1	1	1	1		1	0	1	1		}	110153.604	-0.009
1	1	1	2	1	1	0	1	2	1	}		
1	1	1	1	2	1	0	1	2	2	}	110154.136	-0.001
1	1	1	1	1	1	0	1	2	2	}		
1	1	1	1	2	1	0	1	2	3	}	110154.177	0.001
1	1	1	1	0	1	0	1	2	1	}		
1	1	1	1		1	0	1	0			110155.038	0.004
					o-NH_2D							
1	0	1	0		0	0	0	1			332780.840	-0.003
1	0	1	2	1	0	0	0	1	0			
1	0	1	2	1	0	0	0	1	1	}	332781.695	0.004
1	0	1	2	1	0	0	0	1	2	}		
1	0	1	2	3	0	0	0	1	2			
1	0	1	2	2	0	0	0	1	1	}	332781.752	0.002
1	0	1	2	2	0	0	0	1	2	}		
1	0	1	1		0	0	0	1			332782.261	-0.006

Notes: Braces denote group of transitions observed as a single line. (a) Omitted when the deuterium hyperfine structure is unresolved. (b) In case of blended transitions, the deviation is computed from their intensity-averaged frequency.

has been improved with respect to Ref. [10] by more than one order of magnitude. Moreover, χ_{aa}(D) and χ_{cc}(D) have been simultaneously determined for the first time, with χ_{cc}(D) being previously derived only from unresolved astronomical spectra [10]. A good agreement between experimental and theoretical values has also to be pointed out.

Even though deuterium hyperfine splittings are quite small and often negligible, it has been shown by

astronomical observations that neglecting them in the line-profile analysis can lead to an overestimation of the NH_2D column density by about 50% [10]. A similar effect is possibly exhibited by other deuterium-bearing species, such as multiply-deuterated ammonia NHD_2 and ND_3, which suffer from the same lack of laboratory data. While a more extended investigation of the rotational spectra of ammonia isotopologues is in progress in our laboratory, the new set of spectroscopic constants determined in this work offers a reliable line-catalog (taking into account both N and D hf splittings) that can be used to guide future astronomical observations of NH_2D.

6. Acknowledgement

This study was supported by Bologna University (RFO funds) and by MIUR (Project PRIN 2015: STARS in the CAOS, Grant Number 2015F59J3R). The work in Mainz has been supported by the Deutsche Forschungsgemeinschaft via grant GA 370/6-2 within the framework of the priority program SPP 1573.

References

[1] A. Cheung, D. M. Rank, C. Townes, D. D. Thornton, W. Welch, Detection of NH_3 molecules in the interstellar medium by their microwave emission, Phys. Rev. Lett. 21 (1968) 1701.
[2] B. A. McGuire, 2018 Census of Interstellar, Circumstellar, Extragalactic, Protoplanetary Disk, and Exoplanetary Molecules, Astrophys. J. Suppl. S. 239 (2018) 17.
[3] C. Ceccarelli, P. Caselli, D. Bockelée-Morvan, O. Mousis, S. Pizzarello, F. Robert, D. Semenov, Deuterium fractionation: The ariadne's thread from the precollapse phase to meteorites and comets today, Protostars and Planets VI (2014) 859–882.
[4] E. Rodriguez Kuiper, B. Zuckerman, T. Kuiper, Deuterated ammonia toward the Orion Nebula, Astrophys. J. 219 (1978) L49–L53.
[5] B. Turner, B. Zuckerman, M. Morris, P. Palmer, Microwave detection of interstellar deuterated ammonia, Astrophys. J. 219 (1978) L43–L47.
[6] M. Olberg, M. Bester, G. Rau, T. Pauls, G. Winnewisser, L. Johansson, A. Hjalmarson, A new search for and discovery of deuterated ammonia in three molecular clouds, Astron. & Astrophys. 142 (1985) L1–L4.
[7] C. Walmsley, W. Hermsen, C. Henkel, R. Mauersberger, T. Wilson, Deuterated ammonia in the Orion hot core, Astron. & Astrophys. 172 (1987) 311–315.
[8] E. F. van Dishoeck, G. A. Blake, D. J. Jansen, T. Groesbeck, et al., Molecular abundances and low mass star formation II. Organic and deuterated species towards IRAS 16293-2422, Astrophys. J. 447 (1995) 760–782.
[9] R. Y. Shah, A. Wootten, Deuterated ammonia in galactic protostellar cores, Astrophys. J. 554 (2001) 933.
[10] F. Daniel, L. Coudert, A. Punanova, J. Harju, A. Faure, E. Roueff, O. Sipilä, P. Caselli, R. Güsten, A. Pon, et al., The NH_2D hyperfine structure revealed by astrophysical observations, Astron. & Astrophys. 586 (2016) L4.
[11] M. Weiss, M. W. P. Strandberg, The microwave spectra of the deutero-ammonias, Phys. Rev. 83 (1951) 567.
[12] P. Thaddeus, L. Krisher, P. Cahill, Hyperfine structure in the microwave spectrum of NH_2D, J. Chem. Phys. 41 (1964) 1542–1547.
[13] S. G. Kukolich, Measurements of hyperfine structure in NH_2D, J. Chem. Phys. 49 (1968) 5523–5525.
[14] F. C. De Lucia, P. Helminger, Millimeter-and submillimeter-wave length spectrum of the partially deuterated ammonias; a study of inversion, centrifugal distortion, and rotation-inversion interactions, J. Mol. Spectrosc. 54 (1975) 200–214.
[15] E. Cohen, H. Pickett, The rotation-inversion spectra and vibration-rotation interaction in NH_2D, J. Mol. Spectrosc. 93 (1982) 83–100.
[16] M. Bester, K. Yamada, G. Winnewisser, S. Urban, The nuclear hyperfine structure of deuterated ammonia, Astron. & Astrophys. 121 (1983) L13.
[17] L. Fusina, G. Di Lonardo, J. Johns, L. Halonen, Far-infrared spectra and spectroscopic parameters of NH_2D and ND_2H in the ground state, J. Mol. Spectrosc. 127 (1988) 240–254.
[18] W. Gordy, R. L. Cook, Microwave Molecular Spectra, 3rd Edition, Wiley, New York, 1984.
[19] I. Shavitt, R. J. Bartlett, Many-body methods in chemistry and physics: MBPT and coupled-cluster theory, Cambridge University Press, 2009.
[20] K. Raghavachari, G. W. Trucks, J. A. Pople, M. Head-Gordon, A fifth-order perturbation comparison of electron correlation theories, Chem. Phys. Lett. 157 (1989) 479–483.
[21] T. H. Dunning Jr., Gaussian Basis Sets for Use in Correlated Molecular Calculations. I. The Atoms Boron through Neon and Hydrogen, J. Chem. Phys. 90 (1989) 1007.
[22] A. Kendall, T. H. Dunning Jr., R. J. Harrison, Electron affinities of the first-row atoms revisited. Systematic basis sets and wave functions , J. Chem. Phys. 96 (1992) 6796.
[23] D. E. Woon, T. H. Dunning Jr., Gaussian basis sets for use in correlated molecular calculations. V. Core-valence basis sets for boron through neon, J. Chem. Phys. 103 (1995) 4572.
[24] A. K. Wilson, T. van Mourik, T. H. Dunning Jr, Gaussian basis sets for use in correlated molecular calculations. VI. Sextuple zeta correlation consistent basis sets for boron through neon, J. Mol. Struct. THEOCHEM 388 (1996) 339–349.

[25] T. Van Mourik, A. K. Wilson, T. H. Dunning Jr, Benchmark calculations with correlated molecular wavefunctions. XIII. Potential energy curves for He_2, Ne_2 and Ar_2 using correlation consistent basis sets through augmented sextuple zeta, Mol. Phys. 96 (1999) 529–547.
[26] J. F. Stanton, J. Gauss, L. Cheng, M. E. Harding, D. A. Matthews, P. G. Szalay, CFOUR, coupled-cluster techniques for computational chemistry, a quantum-chemical program package, With contributions from A.A. Auer, R.J. Bartlett, U. Benedikt, C. Berger, D.E. Bernholdt, Y.J. Bomble, O. Christiansen, F. Engel, R. Faber, M. Heckert, O. Heun, M. Hilgenberg, C. Huber, T.-C. Jagau, D. Jonsson, J. Jusélius, T. Kirsch, K. Klein, W.J. Lauderdale, F. Lipparini, T. Metzroth, L.A. Mück, D.P. O'Neill, D.R. Price, E. Prochnow, C. Puzzarini, K. Ruud, F. Schiffmann, W. Schwalbach, C. Simmons, S. Stopkowicz, A. Tajti, J. Vázquez, F. Wang, J.D. Watts and the integral packages MOLECULE (J. Almlöf and P.R. Taylor), PROPS (P.R. Taylor), ABACUS (T. Helgaker, H.J. Aa. Jensen, P. Jørgensen, and J. Olsen), and ECP routines by A. V. Mitin and C. van Wüllen. For the current version, see http://www.cfour.de.
[27] J. Noga, R. J. Bartlett, The full CCSDT model for molecular electronic structure, J. Chem. Phys. 86 (1987) 7041–7050.
[28] G. E. Scuseria, H. F. Schaefer, A new implementation of the full CCSDT model for molecular electronic structure, Chem. Phys. Lett. 152 (1988) 382–386.
[29] S. A. Kucharski, R. J. Bartlett, The coupled-cluster single, double, triple, and quadruple excitation method, J. Chem. Phys. 97 (1992) 4282–4288.
[30] M. Kállay, MRCC, a generalized CC/CI program, For the current version, see http://www.mrcc.hu.
[31] D. Feller, The use of systematic sequences of wave functions for estimating the complete basis set, Full Configuration Interaction limit in water, J. Chem. Phys. 98 (1993) 7059.
[32] T. Helgaker, W. Klopper, H. Koch, J. Noga, Basis-set convergence of correlated calculations on water, J. Chem. Phys. 106 (1997) 9639.
[33] M. Heckert, M. Kállay, J. Gauss, Molecular equilibrium geometries based on Coupled-Cluster calculations including quadruple excitations, Mol. Phys. 103 (2005) 2109.
[34] M. Heckert, M. Kállay, D. P. Tew, W. Klopper, J. Gauss, Basis-set extrapolation techniques for the accurate calculation of molecular equilibrium geometries using Coupled-Cluster theory, J. Chem. Phys. 125 (2006) 044108.
[35] I. M. Mills, Vibration-rotation structure in asymmetric- and symmetric-top molecules, Vol. 1, 1972, p. 115.
[36] A. A. Auer, J. Gauss, J. F. Stanton, Quantitative prediction of gas-phase ^{13}C nuclear magnetic shielding constants, J. Chem. Phys. 118 (2003) 10407–10417.
[37] C. Puzzarini, G. Cazzoli, M. E. Harding, J. Vázquez, J. Gauss, A new experimental absolute nuclear magnetic shielding scale for oxygen based on the rotational hyperfine structure of $H_2^{17}O$, J. Chem. Phys. 131 (2009) 234304.
[38] A. A. Auer, High-level ab-initio calculation of gas-phase NMR chemical shifts and secondary isotope effects of methanol, Chem. Phys. Lett. 467 (2009) 230–232.
[39] F. F. S. van der Tak, H. S. P. Müller, M. E. Harding, J. Gauss, Hyperfine structure in the J = 1-0 transitions of DCO^+, DNC, and $HN^{13}C$: astronomical observations and quantum-chemical calculations, Astron. astrophys. 507 (2009) 347–354.
[40] T. Helgaker, J. Gauss, G. Cazzoli, C. Puzzarini, ^{33}S hyperfine interactions in H_2S and SO_2 and revision of the sulfur nuclear magnetic shielding scale, J. Chem. Phys. 139 (2013) 244308.
[41] C. Puzzarini, G. Cazzoli, M. E. Harding, J. Vázquez, J. Gauss, The hyperfine structure in the rotational spectra of $D_2^{17}O$ and $HD^{17}O$: Confirmation of the absolute nuclear magnetic shielding scale for oxygen, J. Chem. Phys. 142 (2015) 124308.
[42] G. Cazzoli, V. Lattanzi, J. L. Alonso, J. Gauss, C. Puzzarini, The hyperfine structure of the rotational spectrum of HDO and its extension to the THz region: Accurate rest frequencies and spectroscopic parameters for astrophysical observations, Astrophys. J. 806 (2015) 100.
[43] C. Puzzarini, J. F. Stanton, J. Gauss, Quantum-chemical calculation of spectroscopic parameters for rotational spectroscopy, Int. Rev. Phys. Chem. 29 (2010) 273–367.
[44] P. Pyykkö, Year-2008 nuclear quadrupole moments, Mol. Phys. 106 (2008) 1965–1974.
[45] J. D. Watts, J. Gauss, R. J. Bartlett, Open-shell analytical energy gradients for triple excitation many-body, coupled-cluster methods: MBPT(4), CCSD+T(CCSD), CCSD(T),and QCISD(T), Chem. Phys. Lett. 200 (1992) 1–7.
[46] J. Gauss, K. Ruud, T. Helgaker, Perturbation-dependent atomic orbitals for the calculation of spin-rotation constants and rotational g tensors, J. Chem. Phys. 105 (1996) 2804.
[47] J. Gauss, D. Sundholm, Coupled-cluster calculations of spin-rotation constants, Mol. Phys. 91 (1997) 449–458.
[48] J. Gauss, J. F. Stanton, Perturbative treatment of triple excitations in coupled-cluster calculations of nuclear magnetic shielding constants, J. Chem. Phys. 104 (1996) 2574–2583.
[49] C. Puzzarini, Ab initio characterization of XH_3 (X = N,P). Part II. Electric, magnetic and spectroscopic properties of ammonia and phosphine, Theor. Chem. Acc. 121 (2008) 1–10.
[50] G. Cazzoli, C. Puzzarini, The lamb-dip spectrum of phosphine: The nuclear hyperfine structure due to hydrogen and phosphorus, J. Mol. Spectrosc. 239 (2006) 64–70.
[51] M. Melosso, C. Degli Esposti, L. Dore, Terahertz spectroscopy and global analysis of the rotational spectrum of doubly deuterated amidogen radical ND_2, Astrophys. J. Suppl. S. 233.
[52] M. Melosso, B. Conversazioni, C. Degli Esposti, L. Dore, E. Cané, F. Tamassia, L. Bizzocchi, The pure rotational spectrum of $^{15}ND_2$ observed by millimetre and submillimetre-wave spectroscopy., J. Quant. Spectrosc. Radiat. Transfer 222 (2019) 186–189.
[53] M. Melosso, L. Bizzocchi, F. Tamassia, C. Degli Esposti, E. Canè, L. Dore, The rotational spectrum of ^{15}ND. isotopic-independent Dunham-type analysis of the imidogen radical, Phys. Chem. Chem. Phys. 21 (2019) 3564–3573.
[54] C. Degli Esposti, M. Melosso, L. Bizzocchi, F. Tamassia, L. Dore, Determination of a semi-experimental equilibrium structure of 1-phosphapropyne from millimeter-wave spectroscopy of CH_3CP and CD_3CP, J. Mol. Struct. 1203 (2020) 127429.

[55] G. Cazzoli, L. Dore, C. Puzzarini, The hyperfine structure of the inversion-rotation transition $J_K = 1_0$ of NH_3 investigated by Lamb-dip spectroscopy, Astron. & Astrophys. 507 (2009) 1707–1710.
[56] L. Dore, L. Bizzocchi, C. Degli Esposti, J. Gauss, The magnetic hyperfine structure in the rotational spectrum of H_2CNH, J. Mol. Spectrosc. 263 (2010) 44–50.
[57] W. E. Lamb Jr, Theory of an optical maser, Phys. Rev. 134 (1964) A1429.
[58] L. Dore, Using Fast Fourier Transform to compute the line shape of frequency-modulated spectral profiles, J. Mol. Spectrosc. 221 (2003) 93–98.
[59] H. M. Pickett, The fitting and prediction of vibration-rotation spectra with spin interactions, J. Mol. Spectrosc. 148 (1991) 371–377.